Journal of Applied Physics

Effect of stress and/or field annealing on the magnetic behavior of the $(Co_{77}Si_{13.5}B_{9.5})_{90}Fe_7Nb_3$ amorphous alloy

Cite as: J. Appl. Phys. 97, 034911 (2005); https://doi.org/10.1063/1.1845577
Submitted: 10 June 2004 . Accepted: 05 November 2004 . Published Online: 18 January 2005

C. Miguel, A. P. Zhukov, J. J. del Val, A. Ramírez de Arellano, and J. González

View Online   Export Citation

ARTICLES YOU MAY BE INTERESTED IN

New Fe-based soft magnetic alloys composed of ultrafine grain structure
Journal of Applied Physics **64**, 6044 (1988); https://doi.org/10.1063/1.342149

Origin of the magnetic anisotropy induced by stress annealing in Fe-based nanocrystalline alloy
Applied Physics Letters **86**, 152513 (2005); https://doi.org/10.1063/1.1901807

Stress-induced magnetic and structural anisotropy of nanocrystalline Fe-based alloys
Journal of Applied Physics **108**, 093927 (2010); https://doi.org/10.1063/1.3506538

Lock-in Amplifiers
... and more, from DC to 600 MHz   Watch

AIP Publishing

Effect of stress and/or field annealing on the magnetic behavior of the $(Co_{77}Si_{13.5}B_{9.5})_{90}Fe_7Nb_3$ amorphous alloy

C. Miguel and A. P. Zhukov
Department of Materials Physics, Faculty of Chemistry, University of Basque Country, Universidad del País Vasco/Euskal Herriko Unibertsitatea (UPV/EHU), P.O. Box 1072, 20080 San Sebastián, Spain

J. J. del Val[a)]
Department of Materials Physics, Faculty of Chemistry, University of Basque Country, Universidad del País Vasco/Euskal Herriko Unibertsitatea (UPV/EHU), P.O. Box 1072, 20080 San Sebastián, Spain and Unidad de Física de Materiales, Centro Mixto Consejo Superior de Investigaciones Científicas (CSIC)-Universidad del País Vasco/Euskal Herriko Unibertsitatea (UPV/EHU)

A. Ramírez de Arellano
Faculty of Physics, University of Sevilla, P.O. Box 1065, 41080 Sevilla, Spain

J. González
Department of Materials Physics, Faculty of Chemistry, University of Basque Country, Universidad del País Vasco/Euskal Herriko Unibertsitatea (UPV/EHU), P.O. Box 1072, 20080 San Sebastián, Spain

Variations of coercive field, induced magnetic anisotropy, and saturation magnetostriction constant in $(Co_{77}Si_{13.5}B_{9.5})_{90}Fe_7Nb_3$ amorphous ribbons submitted to stress and/or axial magnetic-field annealing are reported. The annealing was carried out by using the Joule-heating effect (average temperature values of the sample corresponding to the intensity of the electrical current were 273, 378, 409, and 445 °C) and the applied stress and axial magnetic field during the thermal treatments were 500 MPa and 750 A/m, respectively. As a result of these treatments, a uniaxial in-plane magnetic anisotropy, which affects drastically the soft magnetic character of the samples, was developed. © *2005 American Institute of Physics.* [DOI: 10.1063/1.1845577]

I. INTRODUCTION

Amorphous alloys are characterized by the lack of long-range order from both topological and compositional point of views. The macroscopic disorder is thought to be the origin of some outstanding properties of these materials and, in particular, of its magnetic softness. The local disorder is intrinsical to the amorphous microstructure and is achieved during the fabrication process. Nevertheless, it seems likely that some kind of small structural units with radii of less than 20 Å, which cannot be detected by conventional x-ray diffraction techniques, can exist. These units do not fill all the space by a close-packed structure so that they give rise to fluctuations of the local atomic density as well as to variations in the local atomic-bond orientations. Topologically, point- and linelike microstructural defects also contribute to the fluctuating amorphous microstructure. The point to point varying local order gives rise to fluctuating local magneto-elastic anisotropies which arise from the coupling between internal stresses and magnetostriction. Eventually, pair ordering anisotropies also can contribute to the local anisotropies and may determine the magnetization process of these materials.

Concerning the microstructural character of the metallic glasses, it is remarkable that the anelastic behavior, including the anelastic recovery,[1–5] indicates that the structural anisotropy can be induced by the mechanical deformation. During the creep deformation process, a part of the deformation energy can be stored as structural anisotropy, or anelastic polarization, and is released upon annealing under zero stress, causing an anelastic recovery. The creep-induced structural anisotropy is itself also manifested in the creep-induced magnetic anisotropy.[6–9] However, there has been no direct structural observation of the anisotropy due to the anelastic polarization. It is worth to note that Suzuki *et al.*[10] reported on an observation of such atomic-bond-orientational anisotropy. It is well known that a large uniaxial magnetic anisotropy can be induced in metallic glasses by annealing under applied stress and/or magnetic field.[11–15] In contrast to the field-induced anisotropy, the stress- and stress and field induced anisotropy can also be developed by an annealing above the Curie temperature of the alloy.

On the other hand the so-called "nanocrystalline materials," which are systems consisting of two phases (nanocrystalline grains randomly distributed in a soft magnetic amorphous phase), introduced a few years ago, exhibit an outstanding soft magnetic character. Yoshizawa *et al.*[16] reported that the presence of small additions of Cu and Nb in certain amorphous FeSiB-based alloys allowed the creation of a two-phase material by the devitrification of the conventional amorphous alloy after annealing for 1 h in the range between 500 °C and 600 °C (i.e., at temperatures between the first and second crystallization peaks). After the crystallization, such material consists of small nanocrystals (around 10-nm grain size) embedded in the residual amorphous matrix. In addition, the devitrification process of these amor-

a)Electronic mail: wapvaalj@sq.ehu.es

phous alloys (with trademark Finemet) leads to the possibility of obtaining rather different microstructures depending on the annealing parameters as well as on the chemical composition. These materials exhibit extremely high magnetic softness at certain conditions of thermal treatment. Herzer[17] successfully explained this outstanding magnetic softness as related to the ratio of the exchange-correlation length (or domain-wall thickness) L to the orientation fluctuation length of randomly distributed local easy axes (which can be approximated by the average crystallite size D). In fact, the macroscopic magnetic anisotropy averages out (when $L \gg D$) and the domain walls can move without pinning. For some particular compositions and volume-crystallized fractions the average magnetostriction constant vanishes and the magnetoelastic contributions to the macroscopic anisotropy also become negligible.

Continuous efforts to improve the soft magnetic properties of the Finemet alloy have been made by means of modifications of the alloy composition. Müller *et al.*[18] reported that the substitution of Fe by Co decreases the saturation magnetostriction in Finemet-type amorphous alloys. The addition of Co is also expected to be beneficial to the induction of in-plane magnetic anisotropy in ribbons by magnetic-field annealing, because the substitution of Fe with Co is known to be effective in increasing the magnetic anisotropy constant K_u of FeSiB amorphous alloys.[19] A large K_u value can increase the magnetic-resonance frequency, which is advantageous for the good permeability-frequency (μ-f) property in the high-frequency region. However, the addition of Co to Fe-based amorphous alloys significantly influences the crystallization process (e.g., the density number of Cu-enriched clusters decreases with the substitution of Fe atoms by Co ones parallel to a decrease of the density number of the heterogeneous nucleation sites for bcc-Fe primary crystals[20]).

In the present work a microstructural study, carried out by means of differential scanning calorimetry (DSC), x-ray diffraction (XRD), and transmission electron microscopy (TEM), as well as experimental results concerning the induced magnetic anisotropy (K_{in}), changes in the coercive field (H_c), and the evolution of the magnetostriction constant (λ_s) in $(Co_{77}Si_{13.5}B_{9.5})_{90}Fe_7Nb_3$ amorphous alloy submitted to stress and/or field annealing are reported. The aim of the present work is to obtain information on the stress- and stress and field induced anisotropies and their influence on some magnetic and magnetoelastic properties in this interesting amorphous material within its amorphous state and its beginning of the devitrification process.

II. EXPERIMENTAL PROCEDURE

Amorphous ribbons, with the nominal composition mentioned above, were prepared by melt-spinning technique at the Institute of Solid State Physics of Chernogolovka (Russia). Magnetic measurements were carried out onto ribbons of the following dimensions: 3.1 mm wide, 20 μm thick, and 10 cm long. The microstructural character of the samples (in as-quenched and annealed states) was investigated by XRD

and TEM techniques. Consequently, the amorphous character of the as-cast ribbon has been confirmed by both XRD and TEM analyses.

Thermal treatments under a tensile stress of 500 MPa and/or a magnetic field of 750 A/m (applied longitudinally to the ribbon) were carried out by means of the Joule-heating technique on the as-cast (AC) samples. In order to develop a macroscopic magnetic anisotropy, three additional kinds of thermal treatments using current annealing (CA) technique were carried out, namely,

(1) under the simultaneous action of a tensile stress (500 MPa), named SA;
(2) under axial magnetic field (750 A/m), named FA; and
(3) under both, tensile stress (500 MPa) and magnetic field (750 A/m), named SFA

We have previously determined the relationship between the electrical current annealing and the corresponding temperature of the sample as described in Ref. 21. The thermal treatment was carried out at four annealing currents corresponding to 273, 378, 409, and 445 °C, just below (the first one) and above the Curie point (the three other ones), for 120 s. In order to remark on this fact, the Curie point corresponding to the precursor amorphous material, T_C^{am}, was estimated to be around 335 °C.[21] The samples were cooled under the action of the applied stress and/or magnetic field down to room temperature. Thermal analysis of the treated samples was carried out using the DSC technique. The devitrified structures obtained after thermal treatments were put in evidence by the XRD and TEM observations. The grain size distribution has been also determined directly from the TEM micrographs.

In the following we will focus the attention on the changes of the coercive field and the induced magnetic anisotropy produced by these four kinds of treatments. The typical magnetic parameters (coercive field, magnetization, and magnetization work) were deduced from the hysteresis loop measured at room temperature by a fluxmetric method in quasistatic conditions (the maximum applied magnetic field was 5500 A/m). It must be noted that this value of the axial magnetic field must be quite large to approach the magnetic saturation of the different studied samples because of their extremely soft magnetic character as well as of their unidimensionallike character (their length is several orders of magnitude larger than their width and thickness). Consequently, the demagnetizing effects in the longitudinal direction can be considered as negligible. The anisotropy induced in the sample was evaluated from the difference between the magnetization work W_m obtained from the longitudinal magnetization curves measured before and after the treatment. The magnetization work W_m was determined from the longitudinal magnetization curve M_S vs H_z as

$$W_m = \int_0^{M_S} \mu_0 H_z dM_z, \tag{1}$$

where H_z was produced by means of a Helmholtz coilsystem providing a magnetic field of up to 5500 A/m and M_S was evaluated by means of an integration of the electric signal

from a secondary coil surrounding the sample. More details can be found in Ref. 21.

The evaluation of the saturation magnetostriction λ_s was carried out by the small-angle magnetization rotation (SAMR) method. As it has been detailed elsewhere,[22] this method makes use of the variations in the signals $V_{2\omega}$ picked up by a narrow coil when a saturating dc axial field H_z a small ac transverse field H_y and a tensile stress σ_a are simultaneously applied to the sample. The experimental setup described above was used to apply the dc field and the tensile stress, and to detect the induced signal. When a tensile stress σ_a is applied, the induced signal $V_{2\omega}$, measured by a lock-in amplifier, increases or decreases as a consequence of the increment of magnetoelastic anisotropy with a transverse or an axial easy axis, respectively. The change in $V_{2\omega}$ can be compensated by an adequate modification of H_z, so that $V_{2\omega}$ takes the same value as before the stress was applied. In this way, the magnetostriction λ_s is given by

$$\lambda_s = \frac{\lambda_0 M_S}{3} \frac{\Delta H_Z}{\Delta \sigma_a} V_{2\omega} = \text{const.} \qquad (2)$$

The dc axial magnetic field was large enough (up to 7500 A/m) to guarantee the magnetic saturation of the samples. More details on this method can be found in Ref. 23.

Special care was taken to perform all the structural, magnetic, and magnetostriction measurements in the Joule-heated samples, since small differences in the sample cross section or in the annealing history could mask a good correlation between the experimental results. The cross section is a fundamental parameter in the Joule-heating procedure, since it determines the macroscopic resistance and the local power losses during the annealing.

III. EXPERIMENTAL RESULTS AND THEIR ANALYSIS

A. Microstructural analysis

The crystallization process in the samples submitted to the four types of thermal treatments was investigated by DSC technique from 0 up to 700 °C with a heating rate of 20 °C/min. Before these measurements the indium reference was run in order to correctly calibrate the temperature. The results of the samples previously annealed at 273 and 445 °C for 2 min using the four described thermal treatments are plotted in Fig. 1. It must be underlined that the samples treated at 378 and 409 °C show similar DSC plots to the one treated at 273 °C. Therefore, the samples treated at low annealing temperature (273–409 °C) present two peaks of crystallization: the first one, located around 500 °C, can be ascribed to the primary crystallizations, corresponding to the formation of a bcc Fe(Co,Si)-based and bcc Co-based solid solution.[24] In addition, no iron segregations were found during such primary crystallization. The second peak (around 650 °C) corresponds to the bcc to hcp transformation of Co particles such as can be assumed by its sharp shaped. The presence of the two peaks in the DSC curves evidence the absence of crystallization of the samples; this fact must be attributed to the previous stress and/or field annealing which mainly produce a structural relaxation linked to the induction
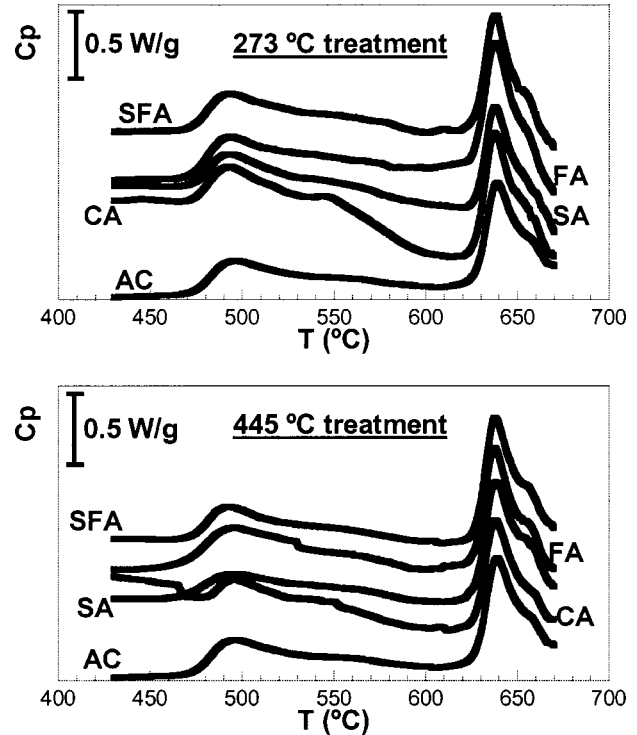

FIG. 1. DSC scans obtained for the different treated samples annealed at 273 and 445 °C. AC: as-cast, CA: current annealing, SA: stress annealing, FA: field annealing, and SFA: stress and field annealing.

of magnetic anisotropy. Besides, we must point out that the DSC curves are very similar in the previously treated samples, indicating that the stress and/or magnetic field acting during the induction treatment seems to be almost irrelevant for the crystallization processes.

The DSC study denotes that the substitution of Fe by Co causes a decrease of the crystallization temperature and, consequently, decreases the thermal stability of the amorphous alloy and resulting in a grain growth. In addition, the DSC curves of the samples treated at high temperature (445 °C) roughly allows to distinguish the first peak, disappearing for the SA and SFA samples. This should be ascribed to the nanocrystallization process occurring at this high temperature, the action of the applied tensile stress being more favorable to develop such process.

Figure 2 shows the XRD patterns of the as-cast and treated (409 °C and 120 s) samples as an example of the structural variations induced by the above described treatments. All the diffraction patterns have been normalized in the high q-range where the intensity cannot vary between the different samples owing to the very short structural distances responsible for the scattering in this q region. It is obvious that the treated samples, in comparison to the as-cast one, show a scattering excess which can be attributed to a crystalline peak overlapping on the amorphous halo, corresponding to the crystallization of bcc-Co phase.[25] The evaluation of the crystalline phase formed with the treatment has been made by means of a substraction of the amorphous halo of the pattern of the as-cast sample (see an example in Fig. 3). The normalization to the total intensity constitutes the crys-
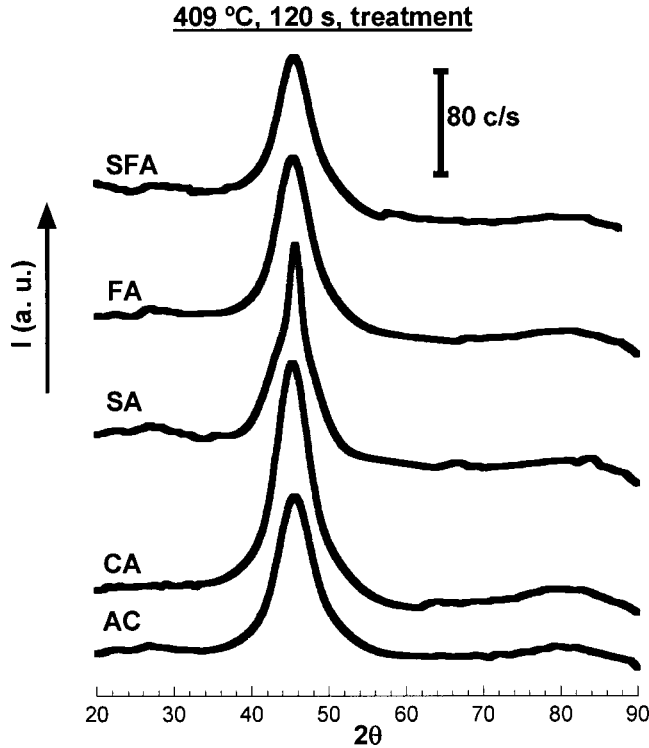
409 °C, 120 s, treatment

FIG. 2. XRD patterns in the sample submitted to different treatments. AC: as-cast, CA: current annealing, SA: stress annealing, FA: field annealing, and SFA: stress and field annealing.

tallinity ratio (χ), which is widely used to characterize semicrystalline materials such as semicrystalline polymers,[26] defined as following:

$$\chi = \frac{\int q^2(I - Ia)dq}{\int q^2 Idq}, \tag{3}$$

where I and Ia, respectively, denote the total scattered intensity by the sample and the intensity of the amorphous reference and q is the scattering vector ($q = 4\pi \sin \theta / \lambda$). The obtained values of χ strongly depend on the temperature, time, and type of the treatment. In any case, the results indicate that, for a given type of treatment, the higher the temperature and the time, the higher the obtained χ value. For CA treat-
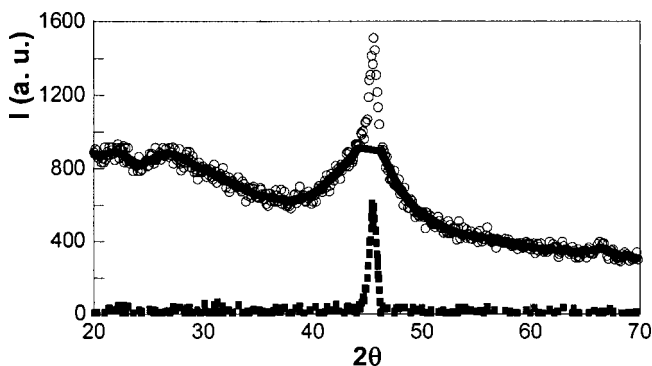
FIG. 3. XRD pattern obtained in the sample treated at 445 °C for 450 s. The continuous line denotes the amorphous background and the dashed line is the remaining scattering of the crystallized phase.
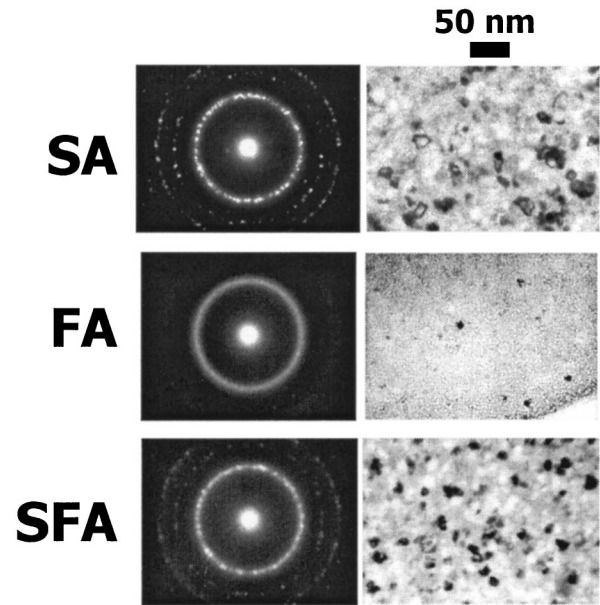

FIG. 4. TEM patterns and images obtained for the sample annealed at 409 °C for 120 s and SA, FA, and SFA treated.

ment at 409 °C for 120 s the sample is 17% crystallized and at 445 °C for 450 s the obtained crystallized phase is 24%. For SA treatment at 409 °C for 120 s the sample is 13% crystallized, and a SFA treatment at 445 °C for 300 s leads to a χ value of 15%.

The width of the crystalline peak leads to an evaluation of the crystallite size (D) from Scherrer's formula,

$$D \cong \frac{\lambda}{\varepsilon \cos \theta_m}, \tag{4}$$

where $\lambda = 0.154$ nm is the wavelength of the Cu $K\alpha$ radiation used, ε is the half-height width of the peak, and $2\theta_m$ is the angular position of the maximum of the peak. The crystalline peaks obtained in the patterns are narrowed with longer temperatures and times of treatment resulting in crystallite sizes between 10 and 25 nm in the range of temperatures and times used for the treatments. These D values are similar to the ones obtained by TEM, as shown below.

The microstructure of the annealed samples has also been studied by TEM in order to clarify the microscopic mechanisms responsible for the magnetic anisotropy induced by the different thermal treatments. Figure 4 shows TEM bright field micrographs of the samples annealed under thermal parameters (time and temperature) which develop the maximum of induced magnetic anisotropy as it will be presented in Sec. III B. bcc-Fe(Co,Si) and bcc-Co phases and a residual amorphous phase were detected in the SA and SFA samples, while the FA samples presents an amorphous state with some clusters dispersed randomly in the amorphous matrix. This microstructure of the FA sample is typically observed in the Finemet alloy annealed around 450 °C (preprimary crystallization) because of the formation of a high number of Cu-enriched clusters that serve as heterogeneous nucleation sites for bcc-Fe particles.[27] Figure 5 shows the grain size distribution obtained for the SA and SFA samples corresponding to the microstructures shown in the Fig. 4. As
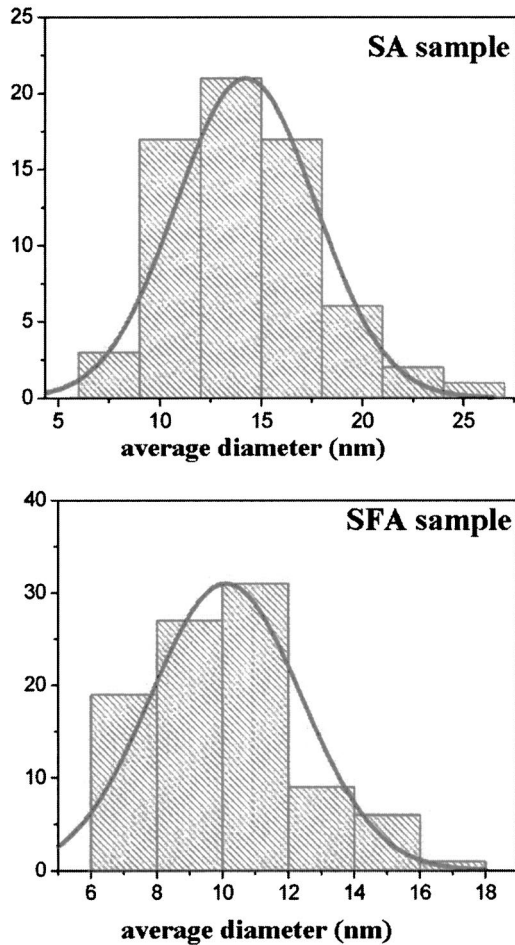
FIG. 5. Grain size distribution obtained from TEM data for the SA and SFA samples annealed at 409 °C for 120 s.

it can be seen, a rough fitting allows to estimate that the mean grain size of the SA sample ($\approx 14.2 \pm 0.4$ nm) is significantly larger than that of the SFA sample ($\approx 10.1 \pm 0.2$ nm); this fact could indicate, as it has been mentioned, that the primary crystallization is hindered by the nanocrystallization occurring due to the heterogeneous nucleation mechanism in the SFA sample owing to the presence of the magnetic field during the thermal treatment.

The TEM investigations, which can be considered as confirmed with the XRD data, have revealed that the dimensions of the stable grains are in the nanometric scale like similar soft magnetic alloys such as Finemet or Nanoperm, widely studied, where spherical bcc-Fe nanoparticles (with dimensions between 5 and 20 nm) randomly distributed are crystallized. It seems that the diffusion field impingement limiting the bcc crystalgrowth[28,29] (effect of Nb and B atoms at the interface nanoparticle-amorphous matrix and Cu clustering) does not occur in the alloy studied.

B. Induced magnetic anisotropy and coercivity

Figure 6 shows the hysteresis loops of the as-cast sample and the differently treated (SA, FA, and SFA) onces at 409 °C. The typical soft magnetic character of the as-quenched sample is evidenced from its hysteresis loop (large reduced remanence and very small coercive field). The incli-
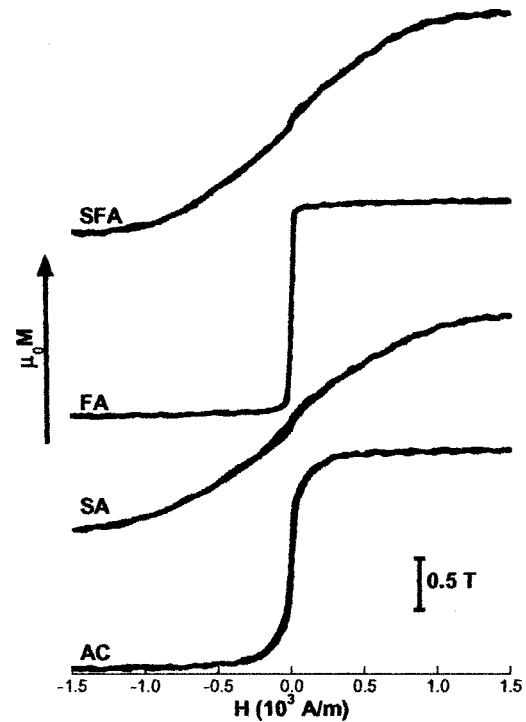

FIG. 6. Hysteresis loops obtained of the as-cast (AC) and the differently treated (SA, FA, and SFA) samples annealed at 409 °C for 120 s.

nation of the hysteresis loop shape of the stress annealed sample indicates that a transverse anisotropy was homogeneously developed by this kind of thermal treatment.

Figures 7 and 8 show the evolution of the coercive field and the induced magnetic anisotropy as a function of the
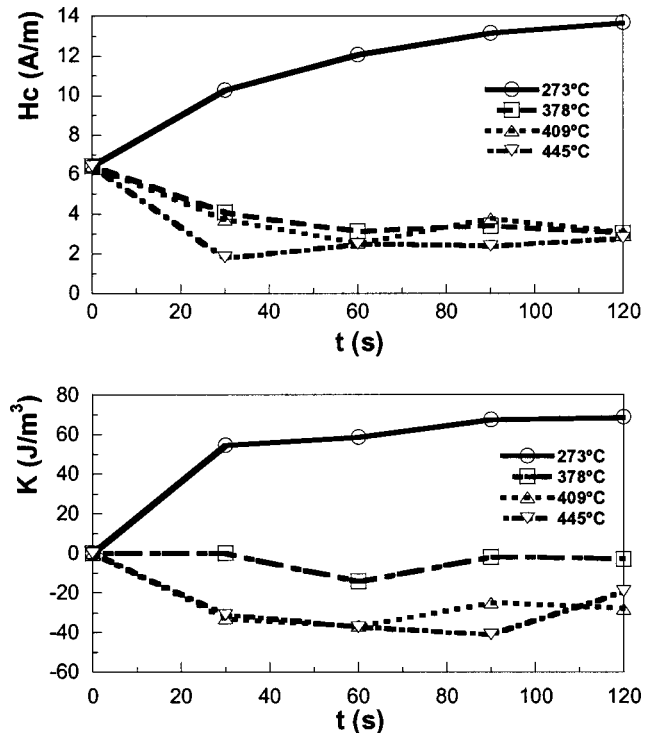

FIG. 7. Annealing time variation of the coercive field (H_c) and the induced magnetic anisotropy (K) at different current densities corresponding to the expressed temperatures for the different current-annealed (CA) samples.
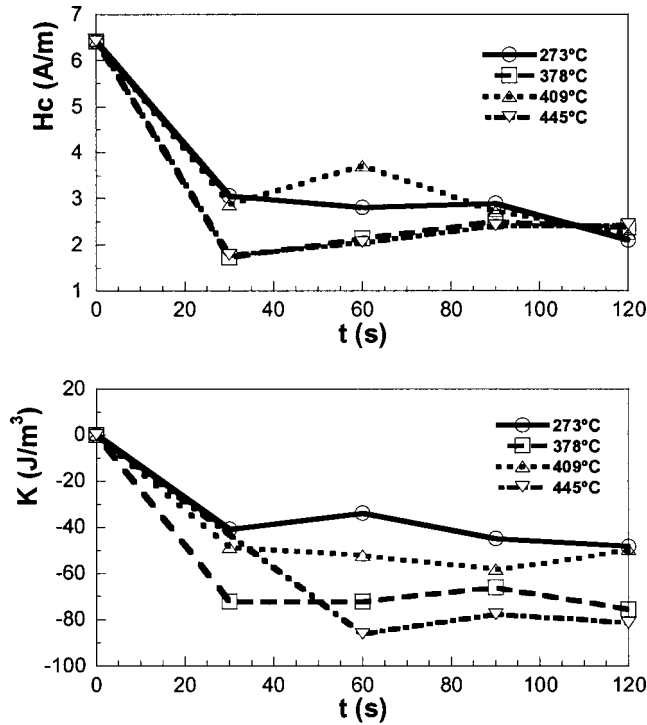
FIG. 8. Variation of the coercive field (H_c) and the induced magnetic anisotropy (K) with the annealing time at different current densities corresponding to the expressed temperatures for the different field-annealed (FA) samples.

FIG. 9. Variation of the coercive field (H_c) and the induced magnetic anisotropy (K) with the annealing time at different current densities corresponding to the expressed temperatures for the different stress-annealed (SA) samples.

annealing time for, respectively, CA and FA samples with the annealing temperature T_{ann} as a parameter. As it is expected, the FA treatment induces longitudinal anisotropy which could simultaneously produce a magnetic softness (put in evidence by a decrease of the coercive field), the magnetization process being mainly caused by a displacement of the domain walls. In this case, a mechanism of atomic-pair ordering could be ascribed for the origin of this field magnetic anisotropy.

The stress annealing treatment develops a magnetic anisotropy with the easy axis transverse to the ribbon axis; this fact implies that the magnetization process is mainly due to the magnetization rotation at large applied magnetic fields. Figure 9 presents the evolution of H_c and K_{ind} with the annealing time for the SA samples, t_{ann}, (with the annealing temperature as a parameter). As it can be seen, the stress-induced anisotropy increases monotonically with the annealing time reaching a maximum, K_{max}, after an annealing time t_{max}. This t_{max} value decreases with the annealing temperature T_{ann}. Such decreasing should be ascribed to the activation of mechanisms, which are in competition with the induction of magnetic anisotropy. Therefore, the maximum of the stress-induced anisotropy for each isothermal treatment can be considered as a "maximum value," K_{max}. It must be noted that the small values of the coercive field for the treatment at 273 °C, which should be ascribed to the structural relaxation of the amorphous phase, is predominant to the nearly zero transverse-induced anisotropy at this low annealing temperature. It must also note that the values of H_c obtained at the highest annealing temperature of 445 °C (around 4−6 A/m) are quite similar to those reported for
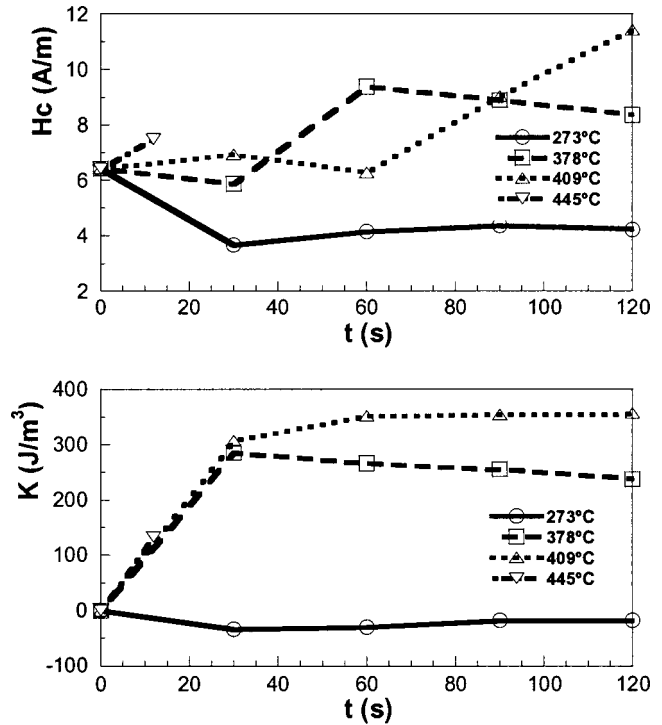
Co-rich amorphous alloys relaxed by the current-annealing technique.[30] Similar remarks can be inferred from the experimental results (variation of coercive field and induced anisotropy) originated by the SFA treatment (Fig. 10).

The evolution of K_{max} as a function of the annealing temperature for the three kind of thermal treatments is shown in Fig. 11. We can observe that the K_{max} value corresponding to SA and SFA increases with the annealing temperature up to a maximum value, which may be roughly related to a maximum of the coercive field. The increase of K and H_c at higher temperatures (up to 409 °C) could be ascribed to a rise in the value of the intensity of the interactions between the metallic atoms and, consequently, an increase of the induced anisotropy could be expected. This argument is linked to the internal stress relaxation produced by thermal treatment in the metallic glasses. Similarly, K_{max} for the FA treatment decreases with the current density down to minimum value. Such minimum is observed again at around 400 °C. For an annealing temperature higher than that of the maximum, K_{max} monotonically decreases with T_{ann}.

We present in Fig. 12 the maximum values of the coercive field (H_c^{max}) achieved at each treatment as a function of the annealing temperature. These maximum values of coercivity are obtained for the same annealing time as the maximum of induced anisotropy given in Fig. 8. As it can be seen, the evolution of H_c^{max} with the annealing temperature results to be quite similar to the one of the stress-induced anisotropy (at least with significant differences between the CA and FA, with respect to SA and SFA treatments). Therefore, a correlation between the coercive field and the stress-induced anisotropy seems to be implied in this stress-annealed alloy.
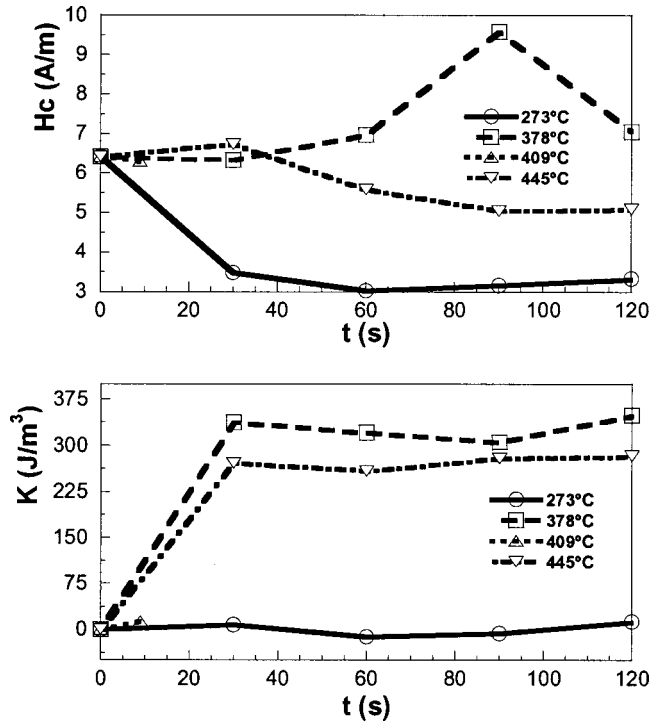
FIG. 12. Variation of the maximum coercive field (H_c^{max}) vs the annealing temperatures of the CA, FA, SA, and SFA samples for 2 min.

fact, Ohnuma *et al.*[32] obtained values of the elongation parallel to the tensile stress which almost agreed with the expected values based on the magnetoelastic and pair ordering models as described in previous studies.[35,36]

C. Saturation magnetostriction

The evolution of the saturation magnetostriction constant as a function of the thermal treatments is presented in Fig. 13. Small values of λ_s (around 2×10^{-6}–6×10^{-6}) are expected for this amorphous alloy and such evolution should be explained taking into account the coexistence of two magnetostrictive phases of different signs with a relative maximum around 420 °C (except for the CA sample). The changes of λ_s below such temperature could be ascribed to the relaxation process, while around 420 °C it seems to indicate the first steps of the beginning of the crystallization process.[27,37]

For an annealing temperature above 420 °C, the presence of a small amount of crystal grains could be considered to explain the magnetostrictive behavior. The low effective magnetostriction in the nanocrystalline sample (treated at a high temperature of 445 °C) could be interpreted in a first approximation by assuming a simple superposition of a volumetrically weighted balance among two contributions with negative signs arising from the bcc-FeSi grains (λ_{Fe}^{cr}) and hcp-Co grains (λ_{Co}^{cr}) and with a positive sign form the residual amorphous matrix (λ_s^{am}) according to Ref. 38,

FIG. 10. Variation of the coercive field (H_c) and the induced magnetic anisotropy (K) with the annealing time at different current densities corresponding to the expressed temperatures for the different stress and field annealed (SFA) samples.

On the other hand, the importance of the two-phase system in the nanocrystalline state has been discussed in detail for the Finemet alloy.[9,17,31] As it has been mentioned in the Introduction section, in two-phase system there is a ferromagnetic coupling, which is responsible for the soft magnetic properties, between the amorphous and nanocrystalline phases. This coupling depends on the size of the crystallites, and, specially, on the induced magnetic anisotropy.

Finally, it has been shown that the stress annealing in Finemet alloy causes the distance of the Fe atoms to be elongated along the direction parallel to the tensile stress.[32] Consequently, the magnetic anisotropy induced by stress annealing will appear and the domain wall will array perpendicular to this elongated direction.[32–35] In addition, the structural origin of this anisotropy is mainly in the crystalline phases [α-Fe(Co,Si) and α-Co phases] and not in the amorphous phase, as it was previously suggested by Kraus *et al.*[33] In
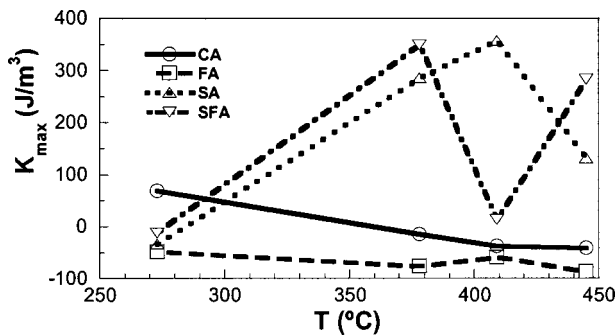

FIG. 11. Variation of the maximum induced anisotropy constant (K_{max}) vs the annealing temperatures of the CA, FA, SA, and SFA samples for 2 min.
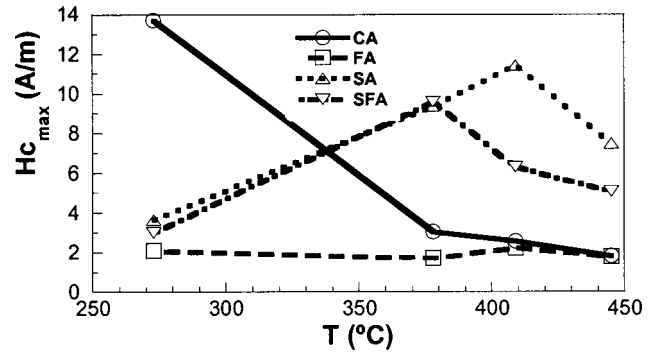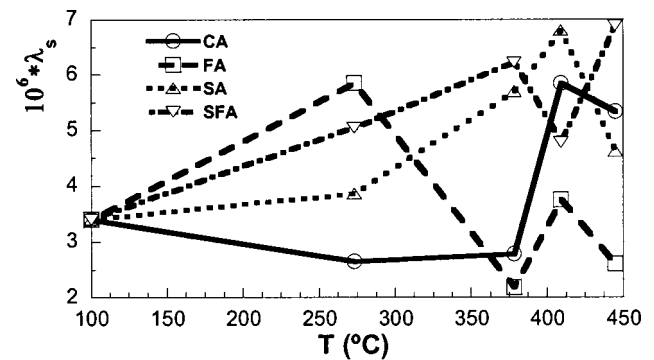

FIG. 13. Variation of the saturation magnetostriction constant (λ) vs the annealing temperatures of the CA, FA, SA, and SFA samples for 2 min.

$$\lambda_s^{\text{ef}} = p_1\lambda_{\text{Fe}}^{\text{cr}} + p_2\lambda_{\text{Co}}^{\text{cr}} + (1 - p_1 - p_2)\lambda_s^{\text{am}}, \tag{5}$$

where $p1$ and $p2$ are the volumetric fraction of the Fe and Co crystalline phases, respectively. Therefore, the variations of λ_s^{ef} can be interpreted as a consequence of the fluctuations of the p parameter. Nevertheless, this approximation ignores the effect of the high density of interfaces. However, the overall behavior of such nanoscale system can be influenced or even dominated by the interfaces. It becomes particularly evident in the case of the interfacial magnetostriction, which could modify the resulting magnetostriction obtained by (5) such as it has been suggested for Fe-based nanocrystalline alloys.[39,40] A deeply microstructural analysis is in progress in order to determine the different parameters (i.e., the fraction volume of the crystalline phases p_1 and p_2, the average radius of the nanocrystals, as well as the thickness of the interfaces) with the final purpose of taking the interface effects into account.

IV. CONCLUSIONS

Changes of the coercive field, induced magnetic anisotropy constant, and variations of the saturation magnetostriction coefficient in $(Co_{77}Si_{13.5}B_{9.5})_{90}Fe_7Nb_3$ amorphous alloy submitted to stress and/or axial magnetic-field annealing are studied (the stress applied during thermal treatment was 500 MPa and the axial magnetic field was 750 A/m). A uniaxial in-plane magnetic anisotropy was developed in the samples as a result of these thermal treatments, which affects drastically the soft magnetic character of the samples.

ACKNOWLEDGMENTS

[1]A. S. Argon and H. Y. Kuo, J. Non-Cryst. Solids **37**, 241 (1980).
[2]A. S. Argon, J. Phys. Chem. Solids **43**, 945 (1982).
[3]N. Morito and T. Egami, Acta Metall. **32**, 603 (1984).
[4]H. R. Hilzinger, in *Proceeding of the 4th International Conference on Rapidly Quenched Metals*, edited by T. Masumoto and K. Suzuki (Japan Institue Metals, Sendai, 1982), p. 791.
[5]H. Szymczak and H. K. Lachowicz, IEEE Trans. Magn. **24**, 1747 (1988).
[6]O. V. Nielsen and H. J. V. Nielsen, J. Magn. Magn. Mater. **22**, 21 (1980).
[7]O. V. Nielsen, H. J. Nielsen, T. Masumoto, and H. M. Kimura, J. Magn. Magn. Mater. **24**, 88 (1981).
[8]T. Jagielinski and T. Egami, IEEE Trans. Magn. **21**, 2005 (1985).
[9]J. González, O. A. Chubykalo, and J. M. González, in *Soft and Hard Magnetic Nanomaterials*, Encyclopedia of Nanoscience and Nanotechnology Vol. 10 (American Scientific Publishers, Baltimore, 2004), p. 1.
[10]K. Suzuki, J. Haimovich, and T. Egami, Phys. Rev. B **35**, 2162 (1987).
[11]O. V. Nielsen, A. Hernando, V. Madurga, and J. M. González, J. Magn. Magn. Mater. **46**, 341 (1985).
[12]O. V. Nielsen, IEEE Trans. Magn. **21**, 2008 (1985).
[13]H. Kronmuller, Phys. Status Solidi B **118**, 661 (1983).
[14]M. Vázquez, E. Ascasibar, A. Hernando, and O. V. Nielsen, J. Magn. Magn. Mater. **66**, 37 (1987).
[15]J. González and K. Kulakowski, J. Magn. Magn. Mater. **82**, 94 (1989).
[16]Y. Yoshizawa, S. Oguma, and K. Yamauchi, J. Appl. Phys. **64**, 6044 (1988).
[17]G. Herzer, IEEE Trans. Magn. **26** (1990).
[18]M. Müller, H. Grahl, N. Mattern, U. Kuhn, and D. Schnell, J. Magn. Magn. Mater. **160**, 284 (1996).
[19]H. Fujimori, H. Morita, Y. Obi, and S. Ohta, in *Amorphous Magnetism II*, edited by R. A. Levy and R. Hasegawa (Plenum, New York, 1977) p. 393.
[20]M. Ohnuma, D. M. Ping, T. Abe, H. Onodera, K. Hono, and Y. Yoshizawa, J. Appl. Phys. **93**, 9186 (2003).
[21]M. Vázquez, J. González, and A. Hernando, J. Magn. Magn. Mater. **53**, 323 (1986).
[22]K. Narita, J. Yamasaki, and H. Fukunaga, IEEE Trans. Magn. **16**, 435 (1980).
[23]A. Hernando, M. Vázquez, V. Madurga, E. Ascasibar, and M. Liniers, J. Magn. Magn. Mater. **61**, 39 (1986).
[24]A. Serebryakov, V. Sedkh, V. Stelmukh, and N. Nvokhatskaya, Nanostruct. Mater. **5**, 519 (1996).
[25]Y. Yoshizawa, J. Metastable Nanocryst. Mater. **1**, 89 (1999).
[26]L. E. Alexander, *X-ray Diffraction Methods in Polymer Science* (Krieger, Malabar, FL, 1985).
[27]M. Vázquez, P. Marin, H. A. Davies, and A. O. Olofinjana, Appl. Phys. Lett. **64**, 3184 (1994).
[28]A. R. Yavari and D. Negri, Nanostruct. Mater. **8**, 969 (1997).
[29]C. Foley, D. R. Allen, and J. H. Perepezko, Mater. Sci. Eng., A **226/228**, 569 (1997).
[30]J. González, M. Vázquez, J. M. Barandiarán, and A. Hernando, J. Phys. D **21**, 162 (1988).
[31]M. E. McHenry, M. Willard, and D. Laughlin, Prog. Mater. Sci. **44**, 291 (1999).
[32]M. Ohnuma, K. Hono, T. Yanai, H. Fukunaga, and Y. Yoshizawa, Appl. Phys. Lett. **83**, 2859 (2003).
[33]L. Kraus, K. Zaveta, O. Heczko, P. Duhaj, G. Vlasak, and T. Schneider, J. Magn. Magn. Mater. **112**, 275 (1992).
[34]B. Hoffmann and H. Kronmüller, J. Magn. Magn. Mater. **152**, 91 (1996).
[35]H. Fukunaga, T. Yanai, H. Tanaka, M. Nakano, K. Takahashi, and Y. Yoshizawa, IEEE Trans. Magn. **38**, 1 (2002).
[36]G. Herzer, IEEE Trans. Magn. **30**, 4800 (1994).
[37]T. Kulik, D. Bucka, and H. Matyja, J. Mater. Sci. Lett. **12**, 76 (1993).
[38]G. Herzer, Phys. Scr.T **49**, 307 (1993).
[39]A. Slawska. Waniewska, R. Zuberek, and P. Nowicki, J. Magn. Magn. Mater. **157/158**, 147 (1996).
[40]H. Szymczak, R. Zuberek, and J. González, J. Magn. Magn. Mater. **191**, 199 (1999).